C. R. Mecanique 339 (2011) 502–517

Contents lists available at ScienceDirect

Comptes Rendus Mecanique

www.sciencedirect.com

Surface mechanics: facts and numerical models

Adhesive contact in the context of multi-asperity interaction

H. Zahouani [a,*], M. Ben Tkaya [a], S. Mezghani [b], C. Pailler-Mattéi [a,c]

[a] University of Lyon, laboratoire de tribologie et dynamique des systemes, UMR CNRS 5513, ENISE-ECL, 58 rue Jean-Parot, 42000 St Etienne, France
[b] Laboratoire de mécanique et de procèdes de fabrication, EA 4106, arts et metiers ParisTech, rue Saint Dominique, BP 508, 51006 Châlons-en-Champagne cedex, France
[c] University Claude-Bernard Lyon 1, ISPB, laboratoire de biophysique, 69003 Lyon, France

ARTICLE INFO

Article history:
Available online 1 July 2011

Keywords:
Roughness
Adhesion
Slopes
Fractal
3D elastic contact model

ABSTRACT

In order to analyse the scale effect of roughness and adhesion in contact between solids, we introduce in this work a 3D model of elastic contact combined with the adhesive theory. The model of roughness with different fractal dimension is introduced to study the adhesive contact in the elastic state at different length scales.
The results of this study show that the scale of roughness modifies the distribution law of the contact pressure and stiffness. The introduction of the adhesive force and fractal property of roughness clearly shows the combined influence of roughness scale and adhesive force on contact stiffness.

1. Introduction

When two nominally flat surfaces are placed in contact, surface roughness causes contact to occur at discrete contact spots. The sum of the areas of all the contact spots constitutes the real contact area, and for most materials with applied load, this will be only a small fraction of the apparent (nominal) contact area. The real contact area is a function of the surface texture, material properties and interfacial loading conditions. The proximity of the asperities results in adhesive contacts caused by interatomic interactions. When two surfaces move relatively to each other, the friction force is contributed by adhesion of these asperities and other sources of surface interactions. A smaller real contact area results in a lower degree of interaction, leading generally to lower wear.

During the period when two surfaces are in contact, the contact will initially generate only a few points to support the normal load. As the normal load is increased, the two surfaces move closer together, a larger number of higher asperities on the two surfaces come into contact, and the existing contact grows to support the increasing load. Deformation occurs in the region of the contact spots, establishing stresses that oppose the applied load. The mode of surface deformation may be elastic, plastic, or viscoplastic, and depends on nominal normal and shear stresses, surface roughness, and material properties. Tips of surface asperities on solid bodies are sometimes considered to be spherically shaped so that the contact of two macroscopically flat bodies can be reduced to the study of an array of spherical contacts deforming at their tips. Through statistical models developed by Greenwood and Williamson [1], we can predict important trends on the effect of surface properties on the real contact area, their usefulness is very limited because of over-simplified assumptions about asperity geometry and height distributions, and the neglected interactions between the adjacent asperities.

The adhesion phenomenon occurs when two surfaces are pressed together, either under a pure normal force or under combined normal and shear forces. A normal tensile force must be exerted to separate the surfaces. The ratio of the normal force F' required for separation to the normal compressive force F initially applied, is often referred to as the adhesion coefficient μ':

* Corresponding author.
E-mail address: hassan.zahouani@ec-lyon.fr (H. Zahouani).

1631-0721/$ – see front matter
doi:10.1016/j.crme.2011.05.008

$$\mu' = \frac{F'}{F} \tag{1}$$

Proximity of the asperities results in an adhesive joint caused by interatomic attractions. In a broad sense, adhesion is considered to be either physical or chemical in nature [2–8]. A chemical interaction involves covalent bonds, ionic or electronic bonds, metallic bonds, and hydrogen bonds; and physical interaction involves the Van der Waals bonds.

Van der Waals forces are much weaker than that in the molecules that undergo chemical interaction. These forces are always present when two asperities are in close proximity. For two solid surfaces in contact, the interfacial bond may be stronger than the cohesive bond in the cohesively weaker of the two materials. Free surface energy influences adhesive bonds of solids in contact and hence friction and wear. In addition, it determines the nature of the interaction of lubricants with solids. When a bond is formed between two materials (having free surface energies per unit area in air γ_1 and γ_2) in contact, the surface energy of the interface per unit area changes to γ_{12}. Based on early work by Bradley [2], and Bailey [9,10], the work of adhesion or the energy of adhesion per unit area is defined as

$$\gamma_{ad} = \Delta\gamma = \gamma_1 + \gamma_2 - \gamma_{12} \tag{2}$$

$\Delta\gamma$ is equal to a reduction in the surface energy of the system per unit area (always negative), in mJ/m^2 or mN/m. Thus $\Delta\gamma$ represents the energy that must be applied to separate a unit area from the interface or to create new surfaces. For two similar materials, $\Delta\gamma$ becomes the work of cohesion and equals $2\gamma_{12} = 0$. This important thermodynamic relationship is valid for both solid and liquid interfaces. γ is generally called free surface energy for solids and surface tension for liquids. McFarlane and Tabor [11] have reported a good correlation between coefficient of adhesion and γ_{ad}/H_s for metal pairs where H_s is the hardness of the softer metal.

Different works describe the analysis of the elastic contact between a sphere and a flat surface, as a first step in understanding the adhesion of solids. Useful approximations are given by the fracture mechanics or energy balance model described by Johnson, Kendall and Roberts (JKR) [12], and the deformed profile of Derjaguin, Muller and Toporov (DMT) [5]. The JKR approximation assumes a value of the work of adhesion or Dupre adhesion energy. It takes into account the additional deformation near the contact periphery resulting from surface forces, over and above the Hertzian deformation that would be given by the external load alone, and is valid in cases of strong adhesion, large radius and low elastic modulus. In the opposite situation, the DMT approximation applies an arbitrary deformed profile, and the appropriate intermolecular force law is assumed, and the force of attraction outside the contact zone is obtained by integration. A rigorous determination of the contact equilibrium between elastic sphere and plate under surface forces involves computation of the total energy in the systems as a function of the contact radius (JKR). Based on the modified Hertz analysis, the expression for adhesive force and contact radius R at no externally applied force is

$$F_a = \frac{3}{2}\pi\gamma_{ad}R \tag{3}$$

The adhesive force required to pull the sphere and the plate apart. Note that F_a is independent from the elastic modulus. The value of F_a is the same whether the surfaces are initially pressed together with an external force or not. As a result of surface forces, the contact size is larger than the Hertzian value without adhesion and will be finite for zero external force.

The contact analysis extension of a sphere against a flat rough surface in elastic contact can be treated statistically. In an interaction between elastic solids, elastic energy is stored in the asperities as they deform to bring surfaces into intimate contact. If this elastic energy is significant compared to the released surface energy ($\Delta\gamma$), the reduction in free energy is small and the resulting adhesion is small and vice versa. Fuller and Tabor [6] modelled asperity contacts of two rough surfaces following Greenwood and Williamson's approach. Their analysis predicts that the adhesion expressed as a fraction of maximum value (relative pull-off or adhesive force) depends upon a single parameter, called the adhesion parameter θ, which is defined as

$$\theta = \left(\frac{4\sigma_p}{3}\right)\left[\frac{E^*}{\pi R_p^{1/2}\Delta\gamma}\right]^{2/3} \tag{4}$$

where σ_p is the composite standard deviation of the summit heights, and R_P is the composite standard deviation of the mean curvature radii of the summits of the two interacting surfaces. The physical significance of the parameter θ can be seen by considering

$$\theta^{3/2} = \frac{1}{\pi}\left(\frac{4}{3}\right)^{3/2}\frac{E^*\sigma_p^{3/2}}{\pi R_p^{1/2}\Delta\gamma} \tag{5}$$

We note that the denominator is a measure of adhesive force experienced by spheres of radius R_p and the numerator is a measure of the elastic force needed to push spheres of radius R_p to a depth of σ_p into an elastic solid of Young's modulus E. Clearly the adhesion parameter represents the statistical average of competition between compressive forces exerted by the higher asperities that are trying to separate the surfaces and the adhesive forces between the lower asperities that are trying to hold the surfaces together. When the adhesion parameter is small (less than 1) the adhesive factor dominates and adhesion is high, and it is small if the adhesion parameter is large (2 or greater).

In this work we have introduced the effect of the adhesion force and roughness on the contact stiffness during a rough elastic contact with low contact pressure.

In Section 2, local roughness is considered to be a distribution of indenters with spherical or conical geometry under the assumption that there is no interaction of the deformations caused by the multi-contact aspect. The introduction of the adhesion force into each roughness model takes into account the local geometry (curvature radius for spherical geometry and angle at the asperity summit for conical geometry). The aim of both these models is to highlight the interdependence of the contact parameters (total contact force, contact area, contact stiffness) of the local roughness analysis scale with respect to the second derivative for the curvature radius and first derivative for the local slopes. These models make it possible to perform a statistical descriptive analysis of the contact for a given distribution law of the roughness heights; however, they are insufficient to take into account the interaction between asperities and modelling of the deformed surface for an elastic and adhesive contact.

By means of a weak load ($F_n = 20$ mN) indentation test, Section 3 illustrates the combined effect of roughness and adhesion force on the contact stiffness between the asperities of a steel solid and a soft PDMS sample with elasticity modulus of 2.2 MPa.

In order to introduce an elastic model taking account of the interaction of the deformation caused by the multi-roughness contact, the 1D finite element model developed in Section 4 shows the interaction effect with respect to the penetration depth into a soft solid. Extension to a 3D elastic contact is introduced in Section 5 by means of Boussinesq's integral equation. Using bidimensional Fourier transform makes it possible to determine in a deterministic way the total elastic force and contact stiffness. The roughness scale effect on the contact stiffness is studied by introducing fractal surfaces for different values of Hölder's exponent so as to vary the local slope scale. Adhesion is introduced by the consideration into the adhesive force term of the local slopes of asperities for a given depth. This elastic modulus with adhesion is applied to fractal surfaces in Sections 5.3 and 5.4 to study the effect of the roughness scale and adhesion energy on the contact stiffness. Analysing the total force with respect to penetration depth shows the twofold effect of the local slope scale on the contact elastic and adhesive components.

2. Elastic models of multiple asperity contacts

2.1. Contact with spherical geometry of asperities

2.1.1. Dry contact

The treatment of a contact problem between such surfaces is simple: The total force is the sum of all of the equal "summit" forces, which can be calculated using the Hertzian contact theory. The individual "micro" contact areas, and therefore, the total contact area, are in this case $A \approx F^{2/3}$. This contradicts not only direct experiments, but also Amontons' law of friction, according to which the frictional force is approximately proportional to the normal force. Therefore, we expect a somewhat linear increase in the contact area with respect to normal force. The situation changes if we take into account that a real surface is, as a rule, stochastically rough. The simplest method of modelling an irregular surface was proposed in 1966 by J.A. Greenwood and J.B.P. Williamson [1]. In this model the authors assumed that all roughness peaks ("asperities") have the same curvature radius and that the heights of the peaks are stochastically distributed around an average value (Fig. 1). If the contacting peaks are far enough away from each other, then their deformations can be considered independent of each other. Thus, the positions of the peaks, and therefore the exact configuration of the surface, matter little in the contact problem (under the given assumptions). Only the height distribution of the peaks is of importance. We describe the probability density of an asperity to have the maximum height z as $\Phi(z)$. That means that the probability that an asperity has the maximum height in the interval $[z, z + \mathrm{d}z]$ is equal to $\Phi(z)\,\mathrm{d}z$. If the total number of asperities is N_0, then the number of asperities in the interval $[z, z + \mathrm{d}z]$ is equal to $N_0\Phi(z)\,\mathrm{d}z$.

For many technical and natural surfaces, it can be assumed that the heights of the peaks are normally distributed:

$$\Phi(z) = \left(\frac{1}{2\pi\sigma_p^2}\right)^{1/2} \exp\left(\frac{-z^2}{2\sigma_p^2}\right) \tag{6}$$

the value σ_p is the root mean square of the height distribution:

$$\sigma_p = \sqrt{\langle z^2 \rangle} \tag{7}$$

We consider a contact between an elastic body with the described statistical roughness and a rigid plane at a distance h_0 from the middle level, at which the value of zero for the z-axis is assumed (Fig. 1). Under the assumption that one can neglect the elastic interactions between the asperities, all of the asperities with a height $z > h_0$ are in contact with the rigid plane. The "penetration depth" of an asperity with height z is $\delta = z - h_0$. For a single contact, we obtain $a^2 = R\delta$, according to the Hertzian theory. Therefore, the contact area of a single asperity is

$$A_i = \pi a_i^2 = \pi R\delta_i = \pi R(z_i - h_0) \tag{8}$$

the single force is

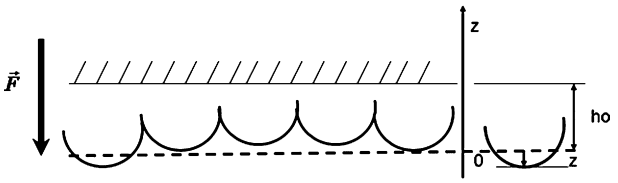

Fig. 1. Stochastic model according to Greenwood and Williamson.

$$F_n^i = \frac{4}{3}E^*\delta_i^{3/2}R^{1/2} = \frac{4}{3}E^*R^{1/2}(z_i - h_0)^{3/2} \tag{9}$$

with

$$\frac{1}{E^*} = \frac{1-\nu_i^2}{E_i} + \frac{1-\nu_s^2}{E_s} \tag{10}$$

E^* is the reduced elastic modulus of the indenter–sample system. E_i and ν_i are Young's modulus and Poisson's ratio of the indenter, and E_s and ν_s are the mechanical parameters of the sample. The total number of contacts, the total contact area, and the total normal force F_n are found through integration over all of the asperities in contact. This means that the integration must be performed over all heights from $z = h_0$ to infinity [1]:

$$N = \int_{h_0}^{\infty} N_0\Phi(z)\,\mathrm{d}z \tag{11}$$

The total area of contact and normal load are respectively given as

$$A_r = N_0\int_{h_0}^{\infty} \pi R(z_s - h_0)\Phi(z_s)\,\mathrm{d}z_s \tag{12}$$

$$F_n = \frac{4}{3}N_0E^*R^{1/2}\int_{h_0}^{\infty}(z_s - h_0)^{3/2}\Phi(z_s)\,\mathrm{d}z_s \tag{13}$$

The average contact pressure is found as [1,13]:

$$\langle\sigma\rangle = \frac{4E^*}{3\pi}\left(\frac{\delta}{R}\right)^{1/2} = \frac{4E^*}{3\pi}\left(\frac{z-h_0}{R}\right)^{1/2} \approx \sqrt{\left(\frac{4E^*}{3\pi}\right)^2\frac{z}{R}} \quad \text{at } h_0 = 0 \tag{14}$$

The curvature radius for an asperity is calculated using $\frac{1}{R} = -z''$. Therefore, for the mean pressure, we get [13]

$$\langle\sigma\rangle = \frac{4E^*}{3\pi}\sqrt{-z.z''} = \frac{4E^*}{3\pi}\sqrt{\langle z'^2\rangle} \tag{15}$$

For the last equation, we have taken into account that the average $-z.z''$ is defined as the integral $\frac{-1}{L}\int_0^L z(x).z''(x)\,\mathrm{d}x$ over a sufficiently large distance L. Partial integration yields $\frac{1}{L}\int_0^L z'(x).z'(x)\,\mathrm{d}x$ and, thus, $\langle z'^2\rangle$.

One can summarise Eq. (15) by using the symbol $\sigma_\theta = \langle z'^2\rangle$ for the root mean square of the slope of the surface profile.

2.1.2. Adhesion effect

During a compressive elastic contact, the energy of the spherical asperity is composed of an elastic contribution and an adhesive contribution. The potential energy for the elastic deformation of the spherical asperity can be calculated with Eq. (16), [13]

$$W_{el} = \frac{1}{2}\int_{\text{Contact area}} p(X).u_z(X)\,\mathrm{d}x\,\mathrm{d}y \tag{16}$$

The form of pressure distribution can be written as

$$p = p_0\left(1 - \frac{r^2}{a^2}\right)^{-1/2} + p_1\left(1 - \frac{r^2}{a^2}\right)^{1/2} \tag{17}$$

The total pressure distribution is the sum of a pressure to produce a homogeneous displacement ($n = -1/2$) and a Hertzian pressure ($n = 1/2$). After the integration of Eq. (16), we obtain the elastic energy as

$$W_{el} = E^*\left[\delta^2 a - \frac{2}{3}\frac{\delta a^3}{R} + \frac{a^5}{5R^2}\right] \tag{18}$$

The total energy is

$$W_{tot} = E^*\left[\delta^2 a - \frac{2}{3}\frac{\delta a^3}{R} + \frac{a^5}{5R^2}\right] - \gamma_a \pi a^2 \tag{19}$$

We obtain the radius at equilibrium a by requiring that the energy of the system assumes the minimum value [12,13]:

$$\frac{\partial W_{tot}}{\partial a} = E^*\left(\delta - \frac{a^2}{R}\right)^2 - 2\gamma_a \pi a = 0 \tag{20}$$

It follows that

$$\delta = \frac{a^2}{R} \pm \sqrt{\frac{2\gamma_a \pi a}{E^*}} \tag{21}$$

Inserting this relationship into (19) provides the total energy as a function of the contact radius [13]

$$W_{tot} = E^*\left[\frac{8}{15}\frac{a^5}{R^2} + \frac{\gamma_a \pi a^2}{E^*} \pm \frac{4}{3}\frac{a^3}{R}\sqrt{\frac{2\gamma_a \pi a}{E^*}}\right] \tag{22}$$

The equation with the minus sign corresponds to the lowest energy state. We obtain the total force acting on the sphere in this state from the derivative of the energy with respect to the displacement δ of the sphere centre [12,13]:

$$F = -\frac{\mathrm{d}W_{tot}}{\mathrm{d}(\delta)} = E^*\left[2\delta a - \frac{2}{3}\frac{a^3}{R}\right] \tag{23}$$

We insert (21) into this equation and obtain the force as a function of the contact radius:

$$F = E^*\left[2\left(\frac{a^2}{R} - \sqrt{\frac{2\gamma_a \pi a}{E^*}}\right)a - \frac{2}{3}\frac{a^3}{R}\right] = E^*\left[\frac{4}{3}\frac{a^3}{R} - \left(\frac{8\gamma_a \pi a^3}{E^*}\right)^{1/2}\right] \tag{24}$$

This force is the sum of elastic (Hertzian force) and adhesive force:

$$F = F_e + F_a \tag{25}$$

with

$$F_e = \frac{4}{3}E^*\frac{a^3}{R} = \frac{4}{3}E^* R^{1/2}\delta^{3/2}$$
$$F_a = -\left(8\gamma_a E^* \pi a^3\right)^{1/2} \tag{26}$$

The maximum negative value of this force is reached when the contact radius a reaches the critical value [13]:

$$a = a_{crit} = \left(\frac{9\gamma_a \pi R^2}{8E^*}\right)^{1/3} \tag{27}$$

and is equal to

$$F_a^{\max} = -\frac{3}{2}\gamma_a \pi R \tag{28}$$

The absolute value of this force is called the adhesive force.

The penetration depth (equation for δ with a minus sign) in the critical state (a_{crit}) is equal to

$$\delta_{crit} = -\left(\frac{3\pi^2 \gamma_a R}{64E^{*2}}\right)^{1/3} \tag{29}$$

On the basis of the statistical approach of Greenwood and Williamson, we can extend this equation to all spherical asperities during a compressive elastic contact, by taking into account the contribution of adhesive force as

$$F_n = \frac{4}{3}N_0 E^* R^{1/2}\int_d^\infty (z_s - h_0)^{3/2}\Phi(z_s)\,\mathrm{d}z_s - \left(8\gamma_a E^* \pi\right)^{1/2} R^{1/3}\int_d^\infty (z_s - h_0)^{3/4}\Phi(z_s)\,\mathrm{d}z_s \tag{30}$$

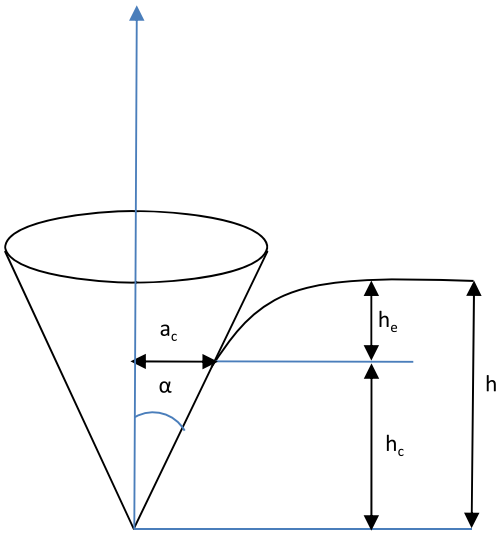

Fig. 2. A schematic representation of a conic asperity tip indenting a half-space sample.

2.2. Contact model with conical geometry of asperities

2.2.1. Dry contact

The proposed analysis of a single conical asperity was developed by L. Sirghi and F. Rossi [14], in nanoscale indentation experiments (tips of AFM probes). This approach introduces the effect of indenter–sample adhesion force in nanoscale indentation experiments. Assessment of elasticity at nanoscale is usually based on Sneddon's solutions of elastic indentation of half-space samples by rigid indenters of arbitrary axis-symmetric profiles. According to Sneddon [15], the stiffness of the axis-symmetric elastic contact, $K_z = \frac{\mathrm{d}F_n}{\mathrm{d}\delta}$, is

$$K_z = 2E^* a_c \tag{31}$$

where F_n is the loading force, δ is the indentation depth, a_c is the radius of indenter–sample contact. Pharr et al. [16] showed that the Sneddon's equation (31) is generally applicable to any axis-symmetric geometry of the indenter–sample contact. If the equation that defines the geometry of the axis-symmetrical indenter, $a_c = f(\delta)$, is known, a_c is determined by the contact depth δ_c (Fig. 2). However δ_c is smaller than the total indenter displacement δ and can be written as [14,16]:

$$\delta_c = \delta - \delta_e \tag{32}$$

With δ_e the elastic displacement of the sample surface at the contact line, it can be determined as

$$\delta_e = \varepsilon\delta \tag{33}$$

where $\varepsilon = 1 - \frac{2}{\pi}$, $\frac{1}{2}$ and 1, for conical, spherical and flat cylinder indenter–sample contact geometry. Combining Eqs. (32) and (33), it follows that [14,16]:

$$\delta_c = (1 - \varepsilon)\delta \tag{34}$$

For the conical indenter–sample contact geometry, δ_c determines the contact radius as

$$a_c = \delta_c \tan\alpha \tag{35}$$

where α is the half cone angle.

2.2.2. Adhesion effect

To take into account the adhesion effect, L. Sirghi and F. Rossi [14] consider that the external loading force applied to the indenter during the unloading process, F_n, is the sum of elastic force of the sample, F_e, and adhesive force F_a:

$$F_n = F_e + F_a \tag{36}$$

Using Sneddon's equation for the elastic force [15], the following equation is found for the elastic stiffness of the indenter–sample contact:

$$\frac{\mathrm{d}F_e}{\mathrm{d}\delta} = \left(\frac{4E^*}{\pi}\right)\tan\alpha\,\delta \tag{37}$$

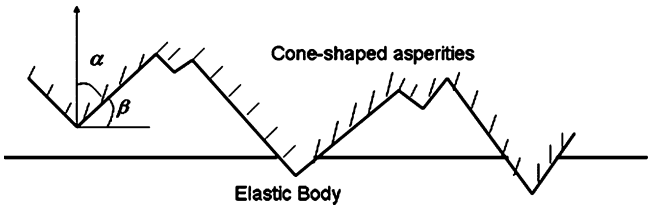

Fig. 3. A schematic representation of multi-asperity contact with a conical morphology indenting an elastic body.

The integral of Eq. (37) gives the pure elastic force for the conical tip–sample contact:

$$F_e(\delta) = \left(\frac{2E^*}{\pi}\right) \tan\alpha . \delta^2 \tag{38}$$

To determine the adhesive force F_a, we can consider the energy of adhesion at the indenter–sample contact as

$$W_a = -\gamma_a A_c \tag{39}$$

where γ_a is the thermodynamic work of adhesion and A_c is the contact area between the indenter and the surface. For the conical geometry, A_c is given as

$$A_c = \frac{\pi \tan\alpha}{\cos\alpha} \delta_c^2 \tag{40}$$

The combination of Eqs. (34), (38) and (39) gives the following expression of the contact adhesion energy [14]:

$$W_a = -\frac{\gamma_a 4 \tan\alpha}{\pi \cos\alpha} \delta^2 \tag{41}$$

Therefore, the adhesive force is

$$F_a = -\frac{\gamma_a 8 \tan\alpha}{\pi \cos\alpha} \delta \tag{42}$$

Finally the external force of the contact is given by [14]:

$$F_n(\delta) = \frac{2E^* \tan\alpha}{\pi} \delta^2 - \frac{\gamma_a 8 \tan\alpha}{\pi \cos\alpha} \delta = F_e(\delta) + F_a(\delta) \tag{43}$$

To extend this equation to the asperities in elastic contact with a smooth plane (Fig. 3), Eq. (44) introduces the average value of asperity cone angles, to determine the total average force in the presence of adhesion.

$$\langle F_n \rangle = \frac{2E^* \delta^2}{\pi} \langle \tan\alpha \rangle - \frac{8\gamma_a \delta}{\pi} \left\langle \frac{\tan\alpha}{\cos\alpha} \right\rangle \tag{44}$$

3. Experimental study

As a case study, we performed indentation experiments on a polydimethylsiloxane (PDMS) surface (thickness of about 4 mm and a Young's modulus of 2.2 MPa), with a textured indenter with a diameter of 2 mm. The 3D morphology and geometrical characteristics (mean cone angle α, and the mean radius of curvature) of cone shaped asperities are given in Fig. 4. We have chosen a PDMS sample for our case study because of its softness and good adhesion to the steel surface of the indenter. Fig. 5 shows the typical force–displacement curve obtained in the micro-indentation experiments on the PDMS sample. The adhesive force effect on the force–displacement curve is easily noticed, as the unloading part of the curve presents an important part with negative values of the unloading force. Fig. 5(A) shows the effect of adhesion for a smooth indenter, while Figs. 5(B), (C) show the simultaneous effect of adhesion (minimum of the negative value of the unloading force) and the mean cone angle on the contact stiffness K_z (N/m).

4. Effect of multi-asperity interaction

To study the effect of multi-asperity interaction, a contact mechanics model between a rough rigid surface and a deformable smooth elastic plane is used. The model can estimate the number of contact asperities, the interaction between different asperities and the resulting surface roughness.

The finite element model was based on rough random surfaces. It is aimed at performing numerical analyses of the surface topography. The need to make the model as simple as possible epitomises the requirement to restrict the problem

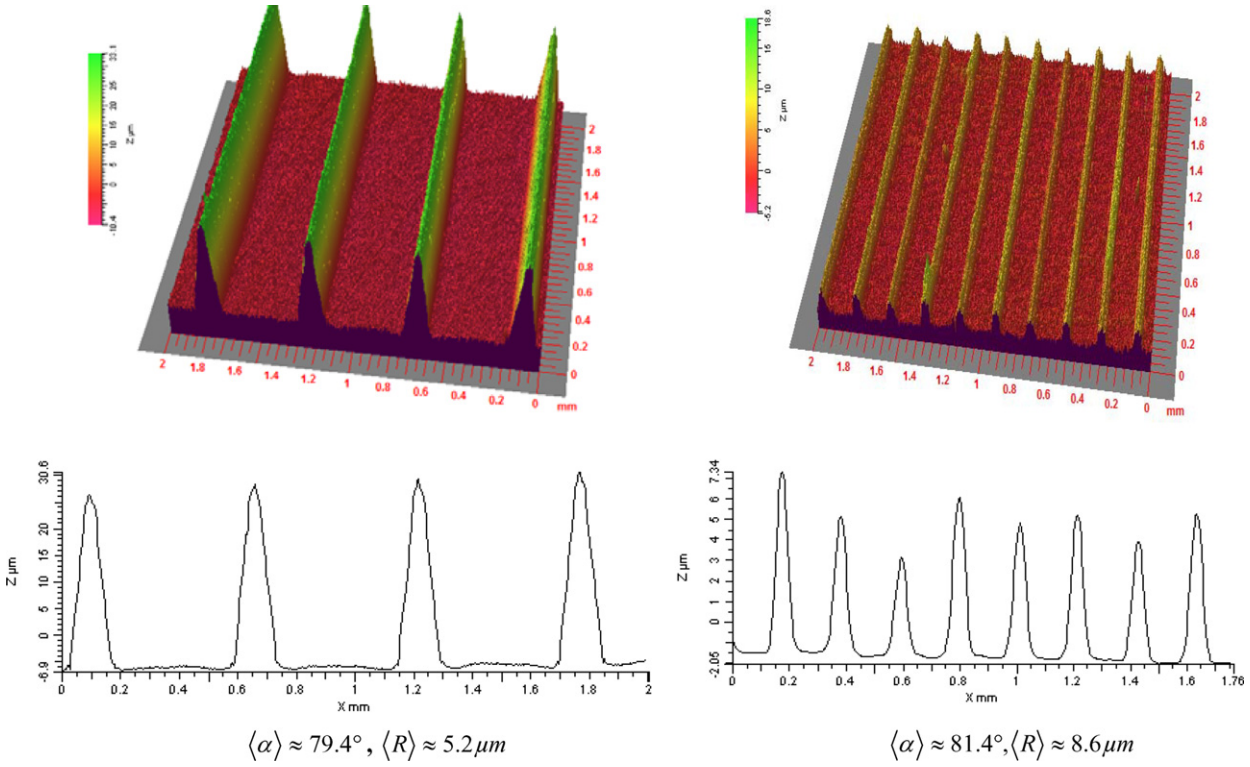

Fig. 4. 3D morphology of textured indenter.

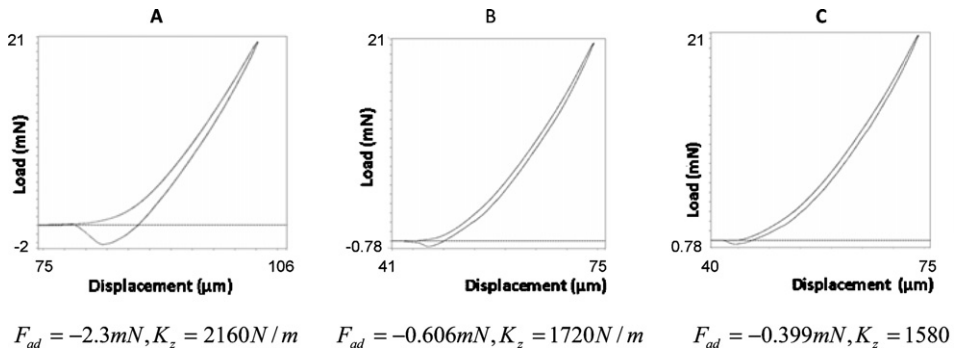

Fig. 5. Experimental indentation with a smooth indenter (A), and textured indenter (B), (C).

to a 2D plane strain finite element model because a detailed finite element model would be very large in the general 3D case.

The interface is presented by means of an elastic deformable flat surface in contact with a rigid rough surface. The major assumptions in the model are:

- The contact between the rough and smooth surfaces resembles the quasi-static indentation of a half space by a hard rigid indenter.
- A 3-node linear plane strain triangle was used to mesh the surface roughness (Fig. 6).
- A 4-node linear plane strain is used to mesh the smooth elastic surface.
- The smooth surface was supposed to be elastic with a Young's modulus equal to 2 MPa.

The output obtained from our model is the resulting roughness and the resulting stress. We notice in Fig. 7 that for a small indentation depth, the grits are barely penetrating into the surface. This leaves untouched areas and there is no interaction between the equivalent stresses. With an increasing penetration of the rough surface, the adjacent grits interact with each other. This interaction influences the distribution of the equivalent Von Mises stress and the topology of the contact area.

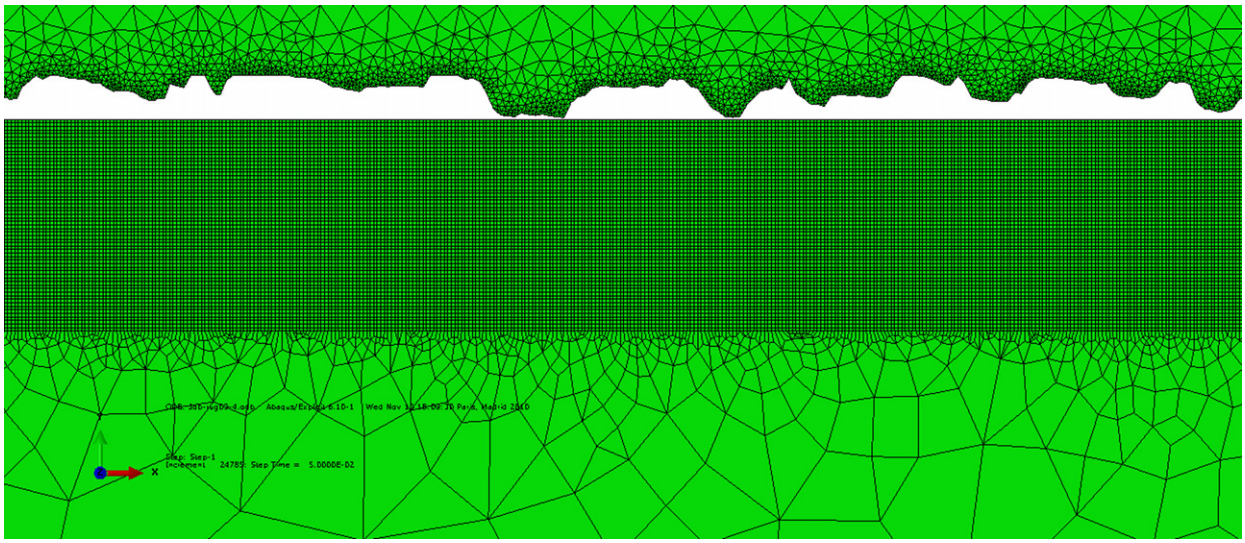

Fig. 6. Mesh used to describe the contact.

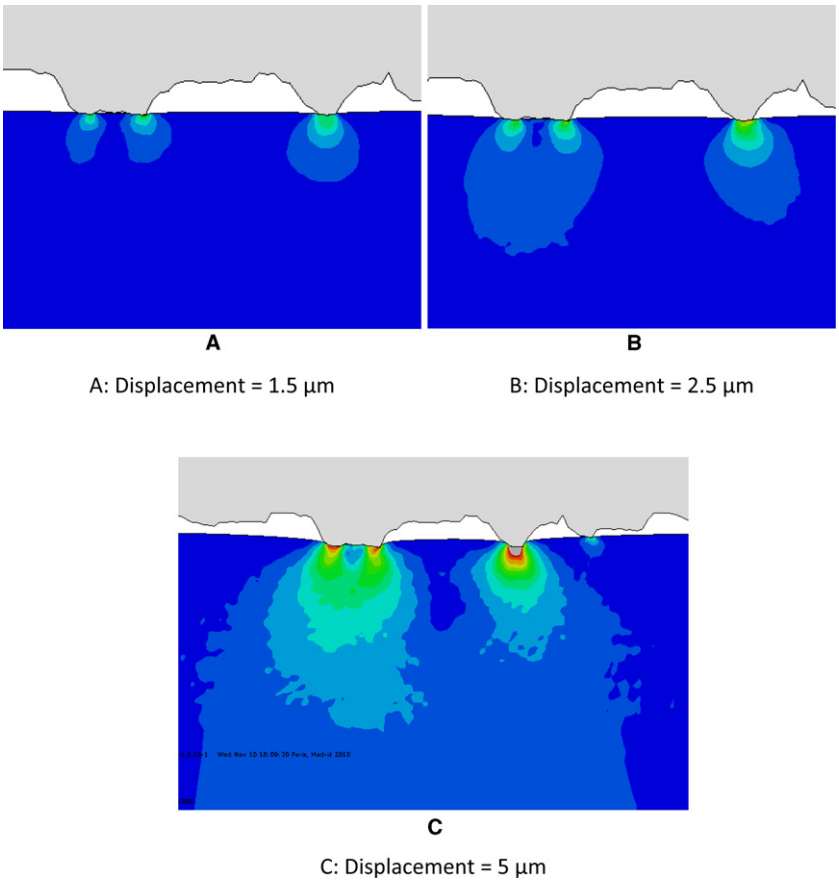

Fig. 7. Effect of multi-asperity interaction.

5. 3D elastic contact model

The characterisation of the roughness multi-scale aspect has shown that slope and curvature are scale dependent, hence the real curvature is not unique [17,18]. Therefore the approximation of asperities as quadratic surfaces is problematic. It has been observed that the roughness parameters used in these models strongly depend on sampling variables describing

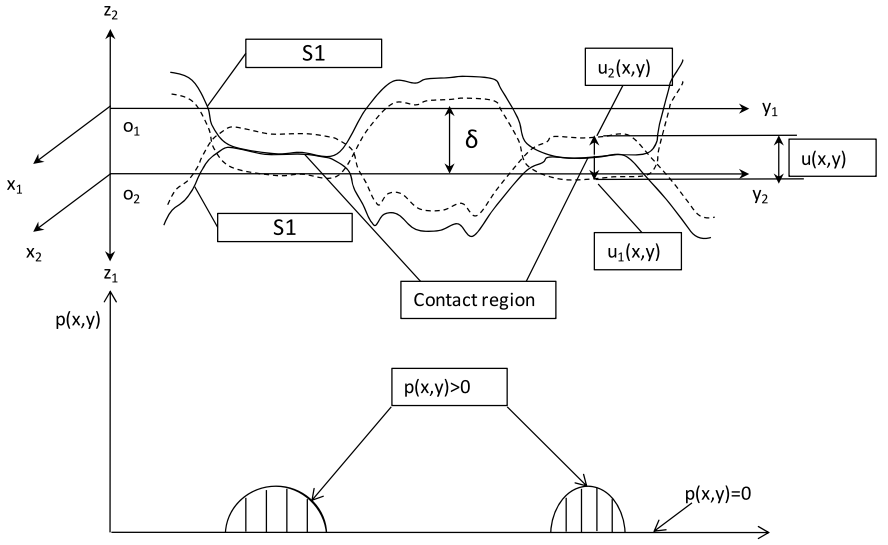

Fig. 8. Schematic representation of multi-contact asperity.

rough surfaces [19,20]. Recently, numerical and semi-analytical models have been developed, allowing the use of digitised real surfaces without any assumption on height distribution or local shape of asperity. However, the grid used to measure the surface must be as fine as possible to capture the roughness in a large scale. In the absence of the ideal sampling of roughness on a wide range of wavelengths and slopes, we chose to work with fractal surfaces statistically self-affined to vary the local slopes in a wide range of scales.

To identify the influence of the roughness scale and adhesion on the elastic contact, we adopted an elastic model allowing us to take full account of interactions between all contact points and to predict the contact geometries of the rough surfaces under load. The problem is treated in the first part of this model by assuming normal effects without the presence of adhesion. In the second part, the model takes into account the adhesive force between surfaces.

If the contact area is small compared to solid dimensions and if slopes of asperities are small everywhere, the solids in contact can be considered as semi-infinite. For the two real surfaces under consideration, the average local mean slope of asperities is smaller than 10°. This remains acceptable for such an approximation. In that case, the elastic displacement of a point M $u(r)$ is linked to the punctual applied load at a distance r by Boussinesq's equation [21]:

$$u(r) = \frac{(1-\nu^2)}{\pi E^* \dots} \frac{F_n}{r} \tag{45}$$

Boussinesq's relationship (45) makes it possible to link the displacement $u_i(x, y)$ of a point $M(x, y)$ of a semi-infinite elastic solid with the contact pressure $p(x', y')$ in $M(x', y')$ related to the contact surface, by means of the following Boussinesq's integral equation:

$$u_i(x, y) = \frac{1-\nu_i^2}{\pi E^*} \iint_{A_c} \frac{p(x', y')\,\mathrm{d}x'\,\mathrm{d}y'}{\sqrt{(x-x')^2 + (y-y')^2}} \tag{46}$$

with A_c the contact surface, E^* is a composite Young's modulus, ν the Poisson's ratio of the surface. So if one calls $u(x, y)$, the difference between the M_1 (x point, y, z_1) of the surface of solid 1 (S1) and the M_2 (x point, y, z_2) of the surface of solid 2 (S2), the geometry enables us to write the following relationship:

$$u(x, y) = u_1(x, y) + u_2(x, y) = \delta - \frac{x^2}{2R_1} - \frac{y^2}{2R_2} = \delta - h(x, y) \tag{47}$$

where $u_1(x, y)$ and $u_2(x, y)$ are relative displacements on the two solids, R_1 and R_2 are the principal curvature radii of the two solids, and $h(x, y)$ is the distance between undeformed surfaces.

When solids are elastic and homogeneous, the influence coefficient $C(x', y')$ can be expressed by the methods of potentials proposed by [20]:

$$C\left(x', y'\right) = \frac{1-\nu^2}{\pi E^*} \frac{1}{\sqrt{(x-x')^2 + (y-y')^2}} \tag{48}$$

To determine the displacement of a point $M(x, y)$ of the surface due to the contact pressure, we have to take into account the superposition of all the actions of the different loads in the contact region. The displacement of a point M_{ij} can be written as [22]:

$$u_{ij} = C_{ijkl} p_{kl} \tag{49}$$

where C_{ijkl} is the influence matrix. The problem is to find a pressure $p_{ij} > 0$ to solve the following contact equation

$$C_{ijkl} p_{kl} + h(x, y) - \delta = 0 \tag{50}$$

$$u_{ij} = \delta - h(x, y), \quad p_{kl} > 0 \text{ within contact area}$$

$$u_{ij} > \delta - h(x, y), \quad p_{kl} = 0 \text{ outside contact area} \tag{51}$$

Contact pressure must also verify

$$\frac{1}{A_c} \iint_{A_c} P(x', y')\, dx'\, dy' = P_A \tag{52}$$

The contact equation (49) can be converted into the spatial frequency domain using Fast Fourier Transform (FFT) techniques. Spectral analysis can be used to determine an algebraic relationship between the surface displacement and the contact pressure on different length scales. In the contact space $R(x, y, z)$, if the pressure is treated as input and displacement as output, then the contact equation can be written as a convolution product [22]:

$$u_{ij} = c_{ijkl} \otimes p_{kl} \tag{53}$$

where $\otimes$ is the convolution product. In the Fourier space, the Fourier transform of the convolution product is given by

$$FT(u_{ij}) = FT(C_{ijkl}).FT(p_{kl}) \tag{54}$$

where FT is the Fourier transform with

$$FT\big(u(x, y)\big) U(\nu_u, \nu_v) = \frac{1}{N} \frac{1}{M} \sum_{k=0}^{N-1} \sum_{l=0}^{M-1} u(x_k, y_l) \exp -2\pi j(\nu_u x_k, \nu_v, y_l) \tag{55}$$

When the problem is converted into the frequency domain, the convolution becomes the product of the input and the transfer function [22]:

$$U(\nu_x, \nu_y) = \frac{2(1 - \nu^2)}{E^* \nu_{x,y}} P(\nu_x, \nu_y) \tag{56}$$

where $\nu_x = \frac{1}{k\Delta x}$ is the spatial frequency in the x direction, $\nu_y = \frac{1}{l\Delta y}$ is the spatial frequency in the y direction, $\nu_{x,y} = \sqrt{\nu_x^2 + \nu_x^2}$ is the spatial frequency of the surface, $1 \leqslant k \leqslant N$; $1 \leqslant l \leqslant N$, N and M are the number of points.

Therefore the transfer function is

$$H(\nu_x, \nu_y) = FT(C_{ijkl}) = \frac{2(1 - \nu^2)}{E_{eq} \nu_{x,y}} \tag{57}$$

Eq. (14) can be written as

$$\frac{E^* \nu_{x,y}}{2(1 - \nu^2)} U(\nu_x, \nu_y) = P(\nu_x, \nu_y) \tag{58}$$

Using the properties of Fourier transforms, we can use the relationships between the displacement and its derivative:

$$FT\left(\frac{\partial^n u(x, y)}{\partial x^n}\right) = (2j\pi \nu_{x,y})^n U(\nu_x, \nu_y) \tag{59}$$

where j is the imaginary unit, and for the first derivative, $n = 1$, Eq. (59) became:

$$\dot{U}(\nu_x, \nu_y) = j2\pi \nu_{x,y} U(\nu_x, \nu_y) \tag{60}$$

Substituting Eq. (56) into Eq. (60), it is interesting to note that the spectrum of contact pressure is proportional to the displacement derivative, so that:

$$P(\nu_x, \nu_y) = \frac{E^*}{j4\pi(1 - \nu^2)} \dot{U}(\nu_x, \nu_y) \tag{61}$$

Eqs. (18) and (19) are important characteristics of the elastic contact problem. They imply that the contact pressure and displacement slope have similar frequency compositions. The contact pressure is computed as the inverse of Fourier transform of the pressure spectrum:

$$p(x, y) = FT^{-1}\left[\frac{E^*}{2(1 - \nu^2)} \nu_{x,y} U(\nu_x, \nu_y)\right] \tag{62}$$

with $p(x, y) > 0$.

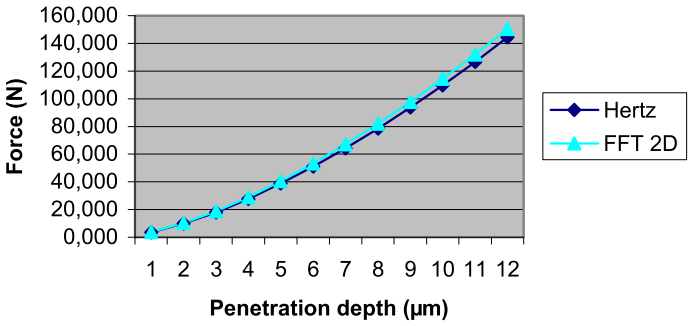

Fig. 9. Force–displacement evolution for Hertz theory and 3D elastic model.

The total load is given as

$$F_n = \sum_i \sum_j p_{ij}(x, y)\Delta x \Delta y \tag{63}$$

The convergence of the general equation is obtained when the relative difference between the external applied load P and computed load F_n is less 10^{-4} [23]:

$$\left| \frac{(P - F_n)}{P} \right| \leqslant 10^{-4} \tag{64}$$

5.1. Validation of the elastic model

To validate the model described above, we apply it to the case of the contact between a smooth sphere and a flat half-space soft material. This validation consists of a comparison of our deterministic model using a spectral approach and Hertz theory.

For normal macroscopic imposed load F, one numerically brings closer two surfaces and solves the equation for each approach level δ. For each normal position δ of the rigid plane, one determines contact pressures $p(x, y)$ by using the direct and inverse Fourier transforms of the contact equations. Convergence is reached when the imposed load is equal to the sum of the local elastic forces calculated:

$$F_n = \sum_i \sum_j p_{ij}(x, y)\Delta x \Delta y \tag{65}$$

The value of the elastic force F_n reached at the convergence for a position δ is compared to the load given by Hertz theory:

$$F_n = \frac{4}{3} E^* \delta^{3/2} R^{1/2} \tag{66}$$

Figs. 10 and 11 show the results of this approach in terms of contact pressure distribution and the deformation of the surface at the maximum of the loading force. We can note the effect of the surface texture on the modification of the Hertzian contact pressure and how the textured surface is deformed elastically.

5.2. Application of multi-scale roughness to fractal model

5.2.1. Self-affined surfaces and modelling of roughness with a large scale of slopes

Our analysis is focused on rough surfaces, whose texture exhibits fractal properties. As shown in many works in the literature [24–28] several machining processes lead to surfaces having this kind of properties. In particular, Majumdar and Bhushan [17,18] reported that processes producing deterministic texture do not yield self-affined fractal surfaces, whereas those producing random textures do. The basic properties of self-affinity are presented in more details in Feder's book [24] and can be defined as below.

A profile $Z(x)$ is self-affined if it is (statistically) invariant under the affined transformation:

$$\left\{ \begin{array}{l} x \to \lambda x \\ Z(x) \to \mu Z(x) \end{array} \right\} \tag{67}$$

the group properties imply that μ should be a homogeneous function of λ. The homogeneity index H such that

$$\mu = \lambda^H \tag{68}$$

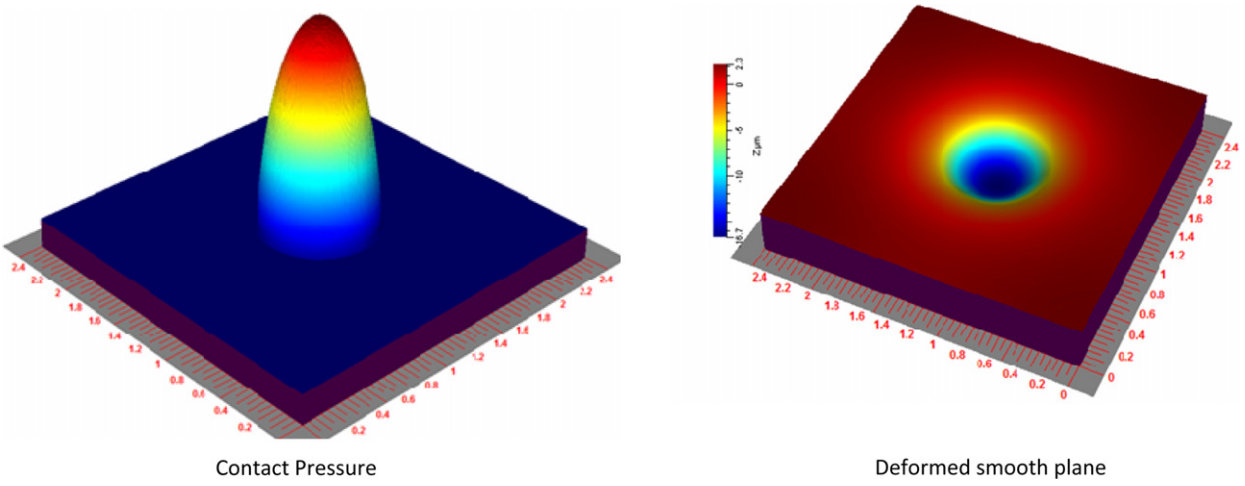

Fig. 10. Contact pressure distribution and deformed elastic surface (sphere/smooth plane).

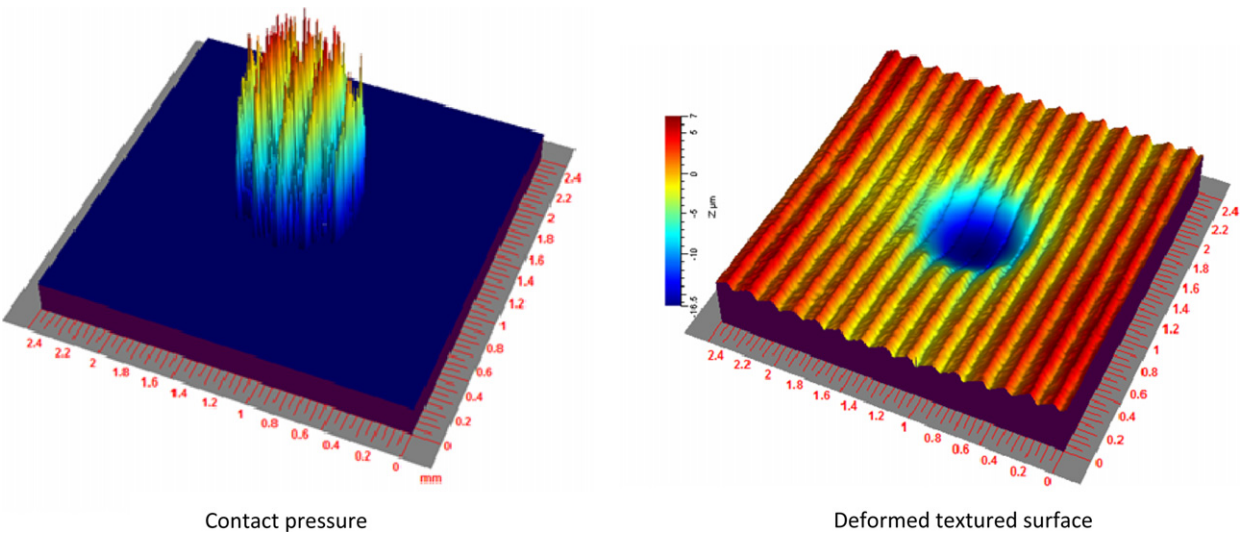

Fig. 11. Contact pressure distribution and deformed elastic surface (sphere/textured surface).

H is the roughness Hurst exponent or Hölder condition, with $0 < H \leqslant 1$. Let us note that for a self-similar invariance, H is the unity. In this case, both scaling factors are equal.

The details of $Z(x)$ depend on the length scale; we assume each realisation of $Z(x)$ to be a continuous, but nondifferentiable function. It means that the presence of any small roughness elements may prevent us from reaching a satisfactory limit of

$$\frac{(Z(x+\Delta)-Z(x))}{\Delta} \quad \text{as } \Delta \to 0 \tag{69}$$

A simple way to obtain this behaviour for a function $Z(x)$ is to assume that the increment of $Z(x)$ is related to Δ by the self-affinity relationship:

$$\left|Z(x+\Delta)-Z(x)\right| \propto \Delta^H, \quad 0 < H < 1,\ \Delta \to 0 \tag{70}$$

This relation can be generalised to dimensions $E > 1$ as follows:

$$\left\langle \left(Z(x+\Delta)-Z(x)\right)^2 \right\rangle \propto \|\Delta\|^{2H}, \quad 0 < H < 1,\ \Delta \to 0 \tag{71}$$

where x represents a point in E-dimensional Euclidean space $\boldsymbol{R}^E$ and $\|\ \|$ stands for the usual norm in this space. This is not a new condition; it is verified for all $\|\Delta\|$ values by the fractional Brownian motions.

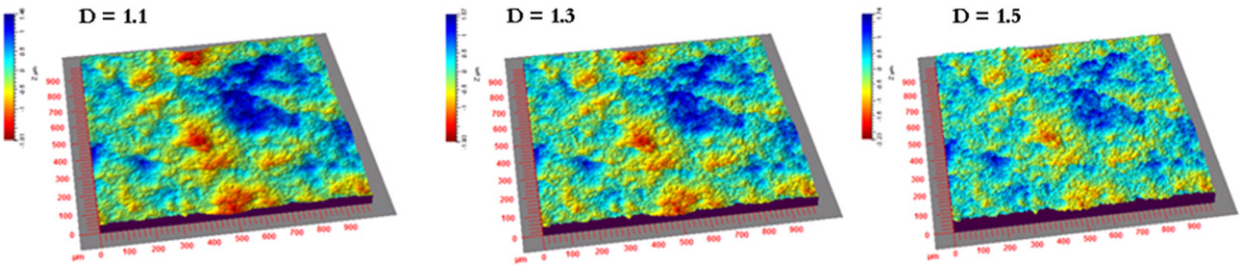

Fig. 12. Fractal surfaces generated with the variation of local slopes.

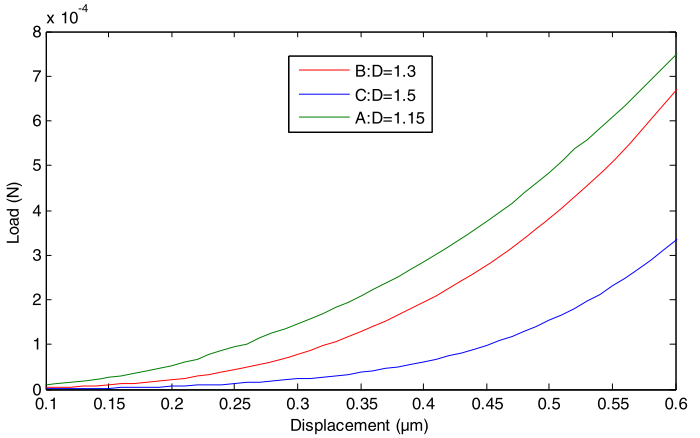

Fig. 13. Effect of fractal dimension on contact stiffness.

5.2.2. Modelling roughness with a large scale of slopes by random midpoint displacement model

For random rough surfaces, the random displacement method used for a fractal profile provides one of the simplest algorithms to generate random fractal surfaces. For analysis proposes, it is particularly useful to have a numerical tool that creates the same kind of morphological data arrays as most scanning acquisition methods for real range images do, namely an x, y array of Z values: $Z(x, y)$. The algorithm of the random displacement method of rough surfaces is used in this work to generate fractal surfaces in a wide range of scales [23,28,29]. Fig. 12 shows a fractal surface generated with this approach, the size of each generated surface is 512×512 points with the steps in the x and y directions of 1 μm.

5.3. Effect of roughness scale on contact stiffness

To study the effect of roughness scale on contact stiffness without adhesion ($\gamma_a = 0$) [23,30–32], we performed a numerical indentation with a 3D elastic model on a polydimethylsiloxane (PDMS) surface (Young's modulus of 2.2 MPa). The texture of the steel indenter is generated with fractal morphology. The procedure of the 3D elastic simulation consists of bringing numerically closer two surfaces and solving the equation for each level of penetration δ. For each normal position δ of the rigid plane, one determines contact pressures $p(x, y)$ by using the direct and inverse Fourier transforms of the contact equations. The step of penetration is chosen as $\delta = 0.01$ μm. The sum of the local efforts calculated for each penetration δ is given as

$$F(\delta) = \sum_i \sum_j p_{ij}(x, y)\Delta x \Delta y \tag{72}$$

In the range of penetration, δ is chosen between 0.01 and 0.5 μm. The fractal dimensions used for this simulation are $D = 1.15$, $D = 1.3$ and $D = 1.5$. Fig. 13 shows the fractal scale effect on the contact stiffness in the absence of adhesive force.

5.4. Effect of roughness scale and adhesive force on contact stiffness

To take into account the adhesion effect on the elastic contact, we introduce the adhesive term of the relationship defined in relationship (44). The total normal load of elastic adhesive contact can be written as follows in this case:

$$F_n = F_e + F_a \tag{73}$$

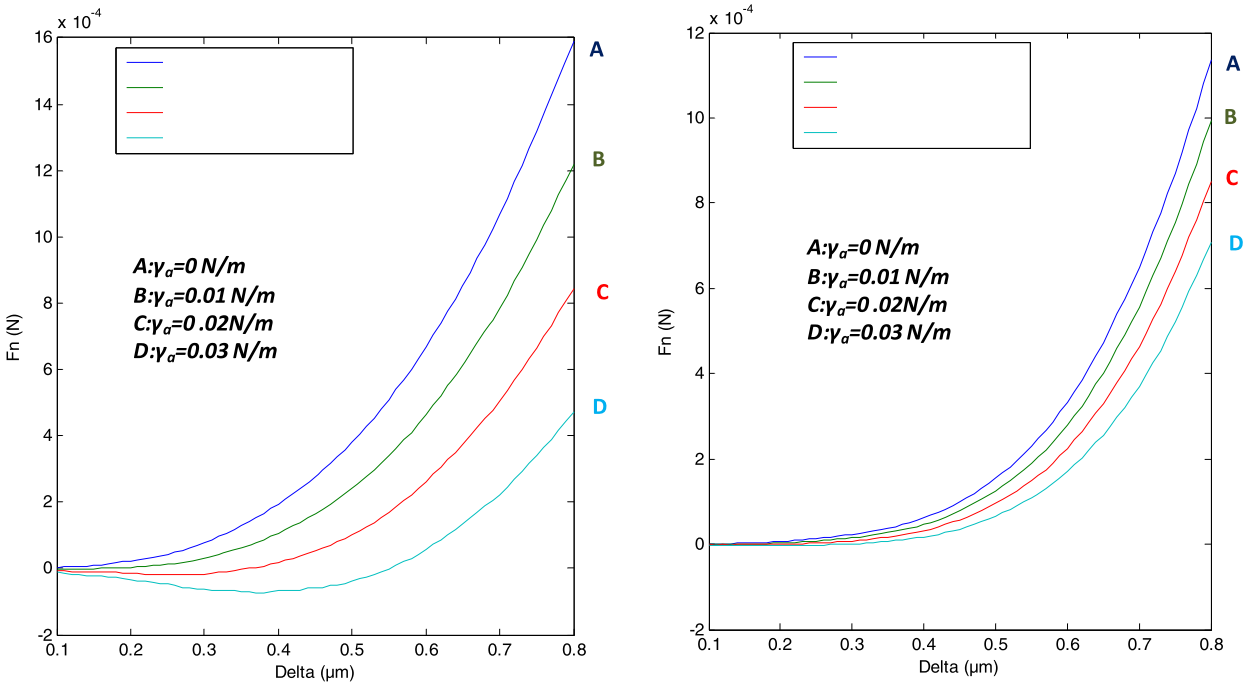

Fig. 14. Effect of adhesion and fractal dimension on contact stiffness.

The total normal load using the 3D elastic model and the adhesion effect can be written for each penetration of a rigid rough plane as a combined elastic and adhesive force:

$$F_n(\delta_k) = \sum_i \sum_j p_{ij}(x, y)\Delta x \Delta y - \frac{8\gamma_a \delta_k}{\pi}\left\langle \frac{\tan\alpha}{\cos\alpha} \right\rangle \tag{74}$$

In the adhesive component, we can notice the effect of the local roughness scale in terms of local slopes where the mean slope value α is computed in the contact region at any depth of penetration δ_k (with k the index of the penetration depth, the step of penetration is chosen as $\delta = 0.01$ μm and the maximum of penetration depth is 0.5 μm). The load–displacement represented in Fig. 14 clearly shows the combined effect of adhesion and fractal roughness on contact stiffness.

6. Conclusions

Due to the multi-scale nature of surfaces, it is found that the surface roughness parameters depend strongly on the resolution of the roughness measuring instrument or any other form of filter, which is not unique for a surface. Therefore, the prediction of the contact models based on conventional roughness parameters may not be unique to a pair of rough surfaces. However, if a rough surface is characterised in such a way that the structural information of roughness at all scales is retained (possible with modern roughness measurement tools like atomic force microscope in large scale), then it will be more logical to use such a characterisation in a contact theory. In order to develop such a contact theory, it is first necessary to quantify the multi-scale nature of surface roughness. Amontons, Coulomb and other early investigations proposed that friction between solids can be attributed to the mechanical interaction of asperities of the contacting surfaces. In the Coulomb model, the action of the wedge-shaped asperities causes the two surfaces to move apart as they slide from one position to another and then come close again. Work is done in raising the asperities from one position to another and most of the potential energy stored in this phase of the motion is recovered as surfaces move back. Only a small fraction of energy is dissipated when sliding down the asperities. Since friction is a dissipative process, the mechanical interaction theory was abandoned. A realistic friction theory should include mechanisms of energy dissipation. Rabinowicz [33] has argued that the real contact area is much larger than that given by deformation as a result of applied load because of the work of adhesion. As the two surfaces come in contact, there is a decrease in the overall surface energy referred to as work of adhesion. Van der Waals forces are always present when two asperities are in close proximity. For two solid surfaces in contact, the interfacial bond may be stronger than the cohesive bond in the cohesively weaker of the two materials. Free surface energy influences adhesive bonds of solids in contact and, hence, friction and wear. In addition, it determines the nature of the interaction of lubricants with solids.

In this work, the adhesive force is introduced in the elastic model of a multi-asperity contact. The combined effect of adhesion and roughness scale modifies the real contact area and consequently the contact stiffness. Force–displacement

curves dependence is described by a sum of two terms: the elastic force computed by the 3D elastic model and a linear term describing the adhesive force. Force–displacement curves with this particular dependence were obtained with this elastic–adhesive model. Surface roughness can have a substantial influence on friction if the adhesive friction is also present. In this case the definition of the friction coefficient must take into account the presence of the adhesive force on the normal force which can modify the prediction of the friction coefficient and lateral stiffness depending on the local roughness scale and adhesive energy. This last point is the objective of the future work based on the contact model developed in this paper.

References

[1] J.A. Greenwood, J.B.P. Williamson, Contact of nominally flat surfaces, Proc. Roy. Soc. A 295 (1966) 300–319.
[2] R.S. Bradley, The cohesive force between solid surfaces and the surface energy of solids, Philos. Mag. 13 (1932) 853–862.
[3] J.J. Bikermann, The Science of Adhesive Joints, Academic Press, New York, 1961.
[4] F.P. Bowden, G.W. Rowe, The adhesion of clean metals, Proc. Roy. Soc. A 233 (1956) 429–442.
[5] B.V. Derjaguin, V.M. Muller, Y.P. Toporov, Effect of contact deformations on the adhesion of particles, J. Colloid Interface Sci. 53 (1975) 314–326.
[6] K.N.G. Fuller, D. Tabor, The effect of surface roughness on the adhesion of elastic solids, Proc. Roy. Soc. Lond. 1 (345) (1975) 327–342.
[7] J.N. Israelachvili, Intermolecular and Surface Forces, 2nd edition, Academic, San Diego, 1992.
[8] W.A. Zisman, Adhesion, Ind. Eng. Chem. 55 (10) (1963) 19–38.
[9] A.I. Bailey, Friction and adhesion of clean and contaminated mica surfaces, J. Appl. Phys. 32 (1961) 1407–1412.
[10] A.I. Bailey, H. Daniels, Interaction forces between mica sheets at small separations, Nature Phys. Sci. 240 (1972) 62–63.
[11] J.S. McFarlane, D. Tabor, Adhesion of solids and the effects of surface films, Proc. Roy. Soc. Lond. A 202 (1950) 224–243.
[12] K.L. Johnson, K. Kendall, A.D. Roberts, Surface energy and the contact of elastic solids, Proc. Roy. Soc. Lond. A 324 (1971) 301–313.
[13] V.L. Popov, Contact Mechanics and Friction, Springer, Heidelberg, Dordrecht, London, New York, ISBN 978-3-642-10802-0, 2010.
[14] L. Sirghi, F. Rossi, Adhesion and elasticity in nanoscale indentation, Appl. Phys. 89 (2006) 243118.
[15] I.N. Sneddon, The relation between load and penetration in the axisymmetric Boussinesq problem for a punch of arbitrary profile, Int. J. Eng. Sci. 3 (1965) 47.
[16] G.M. Pharr, W.C. Olivier, F.R. Brotzen, On the generality of the relationship among contact stiffness, contact area, and elastic modulus during indentation, J. Mater. Res. 7 (1992) 613.
[17] A. Majumdar, B. Bhushan, Fractal model of elastic–plastic contact between rough surfaces, ASME J. Tribology 113 (1991) 1–11.
[18] B. Bhushan, A. Majumdar, Elastic–plastic contact model of bifractal surfaces, Wear 153 (1992) 53–64.
[19] K.L. Johnson, Contact Mechanics, Cambridge University Press, ISBN 0-521-34796-3, 1985.
[20] H. Zahouani, R. Vargiolu, J.L. Loubet, Ph. Kapsa, T.G. Mathia, Effect of lateral resolution on topographical images and 3D functional parameters, Wear (1998) 114–123.
[21] J. Boussinesq, Application des potentiels à l'étude de l'équilibre et du mouvement des solides élastiques, Gauthier–Villars, Paris, 1885, pp. 45–108.
[22] L. Shuangbiao, Q. Wang, G. Liu, A versatile method of discrete convolution and FFT(DC-FFT) for contact analyses, Wear 243 (2000) 101–111.
[23] H. Zahouani, S. Mezghani, C. Pailler-Mattei, M. Elmansori, Effect of roughness scale on contact stiffness between solids, Wear 266 (5–6) (2009) 589–591.
[24] J. Feder, Fractals, Plenum Press, New York, 1988.
[25] B. Mandelbrot, Self-affine fractals and fractal dimension, Phys. Scripta 32 (1985) 257–260.
[26] B. Mandelbrot, J.W. Van Ness, Fractional Brownian motions, fractional noises, and applications, SIAM Review 10 (1968) 422–437.
[27] John C. Russ, Fractal Surfaces, Plenum Press, New York, 1944.
[28] D. Saupe, H.O. Peitgen, The Science of Fractal Images, Springer-Verlag, 1988, pp. 82–91.
[29] H. Zahouani, R. Vargiolu, J.-L. Loubet, Fractal models of surface topography and contact mechanics, Math. Comput. Modelling, Special Issue in Contact Mechanics 28 (4–8) (1998) 517–534.
[30] C. Vallet, D. Lasseux, P. Sainsot, H. Zahouani, Real versus synthesized fractal surfaces: Contact mechanics and transport properties, Tribology International 42 (2) (2009) 250–259.
[31] C. Vallet, D. Lasseux, H. Zahouani, P. Sainsot, Sampling effect on contact and transport properties between fractal surfaces, Tribology International 42 (2009) 1132–1145.
[32] A. Jourani, A. Delalleau, M. Dursapt, F. Sidoroff, H. Zahouani, Effect of local slopes of roughness during contact between solids, Revue Européenne des éléments finis 14 (2–3) (2005) 271–286.
[33] E. Rabinowicz, Friction and Wear of Material, 2nd edition, Wiley, New York, 1995.